Food Chemistry 404 (2023) 134371

Contents lists available at ScienceDirect

Food Chemistry

journal homepage: www.elsevier.com/locate/foodchem

A highly sensitive electrochemical immunosensor based on electrospun nanocomposite for the detection of parathion

Wen-jia Yin [a], Jing-xian Zhang [a], Hong Wang [a,b,*], Yu Wang [c], Xi Zeng [c], Zhen-lin Xu [a], Jin-yi Yang [a], Zhi-li Xiao [a], Bruce D. Hammock [d], Peng Wen [a,b,*]

[a] College of Food Science, Guangdong Provincial Key Laboratory of Food Quality and Safety, South China Agricultural University, Guangzhou 510642, China
[b] Lingnan Modern Agricultural Science and Technology Guangdong Laboratory, Guangzhou 510642, China
[c] Guangzhou Institute of Food Inspection, Guangzhou 510080, China
[d] Department of Entomology and Nematology and UCD Comprehensive Cancer Center, University of California, Davis, CA 95616, United States

ARTICLE INFO

Keywords:
Parathion
Electrospinning
Nanocomposite
Nanobody
Electrochemical immunosensor

ABSTRACT

For monitoring of the residual of parathion pesticide in food, herein, a sensitive and reliable electrochemical immunosensor based on cross-linked polyvinyl alcohol/citric acid nanofiber membrane (PVA/CA NFM) and horseradish peroxidase labeled anti-parathion nanobody was constructed. Firstly, the cross-linked PVA/CA NFM with extra-high surface area and uniform morphology was prepared and characterized. Then, the immunosensor was assembled and its analytical performances were evaluated. It exhibited high specificity and sensitivity to parathion with the liner range and limit of detection being 0.01–100 ng/mL and 2.26 pg/mL, respectively. Moreover, the biosensor kept almost 75% of its initial activity after regenerating 4 times, and remained 85% after 9 weeks of storage. Finally, the average recoveries from food samples were 96.20%–114.61% with the coefficient of variation being 1.06%–5.28%, which was correlate well with UPLC ($R^2 = 0.9964$). Therefore, the sensor was demonstrated to be a feasible alternative for sensitive assay of parathion.

1. Introduction

To increase the production of agricultural commodities, parathion, one of organophosphorus pesticides, has been widely employed in the agriculture field for pest prevention and crop yields guarantee. However, its application has been banned by World Health Organization due to its high toxicity that can deactivate acetylcholinesterase and disturb neuronal system (Liu et al., 2020). In fact, the commercial or other benefits still drive illegal use of parathion in vegetables and fruits (Khairy et al., 2018), especially, it could accumulate in food along with food chain through ecosystem cycle, resulting in health hazards to consumers. Presently, different type of immunoassays, such as gold immunochromatographic assay (GICA) (Liu et al., 2018), indirect enzyme-linked immunoassay (ic-ELISA) (Zhang et al., 2015), chemiluminescence enzyme-linked immunoassay (CLEIA) (Chen et al., 2017) and direct competitive fluorescence enzyme immunoassay (dc-FEIA) (Zhang et al., 2018), have been developed for determination of parathion. However, the sensitivity of GICA cannot meet detecting demand, and the majority of these methods require complicated operating procedures, which limited the on-site application in agricultural products. Hence, it is of great significance and necessity to develop a simple and sensitive method for monitoring of the parathion residual levels.

The immunoassay that combined with electrochemical sensing technology is increasingly considered as a viable alternative to ELISA owing to its higher sensitivity, better specificity and operational simplicity etc. (Jain et al., 2022). Its detection principle is based on changes of electrochemical signals generated by the specific recognition between antigen and antibody, hence, antibody is one of the core components of immunosensor (Felix & Angnes, 2018). Nanobody is a single domain antibody obtained by cloning the variable domain heavy-chain antibodies of *Camelidae* species, possessing preferable properties of small size, elevated solubility, admirable chemical and thermal stability in comparison with conventional antibodies (He et al., 2020). Up to now, nanobody has been applied in the electrochemical immunoassays (Wang & Wang, 2022), for example, the fabricated electrochemical immunosensor using nanobody showed 10-fold sensitivity for detection of Aflatoxin B_1 as compared to that of monoclonal antibody (Pan et al., 2018). Moreover, the nanobody-based electrochemical sensor for Ricin

* Corresponding authors at: College of Food Science, Guangdong Provincial Key Laboratory of Food Quality and Safety, South China Agricultural University, Guangzhou 510642, China.
E-mail addresses: gzwhongd@163.com (H. Wang), pwen@scau.edu.cn (P. Wen).

https://doi.org/10.1016/j.foodchem.2022.134371
Received 28 April 2022; Received in revised form 9 September 2022; Accepted 19 September 2022
Available online 21 September 2022

had better stability at 40°C than the immunosensor based on the conventional monoclonal or polyclonal antibody (Singh et al., 2016). In our previous study, anti-parathion nanobody (VHH9) was prepared with better chemical and thermal stability than prepared anti-parathion monoclonal antibody, and the limit of detection (LOD) of established VHH9-based ic-ELISA and VHH9-alkaline phosphatase fusion protein (VHH9-AP) based dc-FEIA were 1.9 and 0.2 ng/mL, respectively (Zhang et al., 2018), which could be a potential recognition element for electrochemical sensor in the trace levels detection.

Recently, electrochemical immunosensor modified by nanomaterials has been well developed as the nanoscale structure and extra-high surface area could magnify signal response and thus obtain lower detection limit. In which, electrospinning, a relatively simple and facile process to produce nanofiber with high porosity (Wu et al., 2022), is receiving tremendous attention in the field of nanosensor. As the emerging modified electrode material, nanofiber has the following advantages: (1) the ultrahigh surface area can provide more binding sites to increase the loading of immobilized biomolecules; (2) the porous structure is beneficial for analytes diffusing to the interface, facilitating the transfer of electron and thus obtaining faster sensor response (Sapountzi et al., 2017). Immunosensor fabricated by nanofiber exhibited desirable analytical performance (Halicka & Cabaj, 2021). For example, an electrochemical immunosensor for 3-phenoxybenzoic acid was fabricated by covalently immobilizing antigen on the citric acid-decorated nylon 6 nanofiber modified electrode, which showed ultra-high sensitivity with LOD of 0.64 pg/mL and good stability (El-Moghazy et al., 2020). The electrochemical immunosensor based on the polyvinyl alcohol/polyacrylic acid nanofiber mat also possessed high sensitivity towards 19-nortestosterone with LOD of 2.14 pg/mL, a 46-fold times lower compared to the traditional ic-ELISA of pure anti-19-nortestosterone nanobody (Wen et al., 2022). In order to successfully immobilize biomolecules, the nanofibers with rich functional groups and good biocompatibility are needed. Polyvinyl alcohol (PVA) is an inexpensiveness and environmentally-friendly polymer with splendid spinnability, whereas its highly hydrophilic nature restricts its potential as modified electrode material (Mano et al., 2015). In order to ensure the structural integrity of PVA nanofiber, cross-linking with non-toxic crosslinker is more desirable instead of bifunctional aldehydes (Suganthi et al., 2018). Citric acid (CA), an organic acid with three carboxylic acid groups, could react with hydroxyl and amine groups of biopolymers, and thus providing a green way for PVA cross-linking (Sabzi et al., 2020). Moreover, it was reported that cross-linked PVA/CA nanofiber membrane (PVA/CA NFM) possessed considerable carboxylic groups (Lopez-Cordoba et al., 2016; Shi & Yang, 2015), which could be adopted for immobilizing biomolecules, and till now, there is no research on cross-linked PVA/CA NFM as the electrode modification material for electrochemical immunoassay.

Herein, a nanobody-based electrochemical immunosensor with screen-printed carbon electrode (SPCE) that modified by cross-linked PVA/CA NFM was constructed to detect parathion. The cross-linked PVA/CA NFM was prepared and characterized to estimate its potential as modified electrode material. Then, the determination was achieved through a typical competition for binding to horseradish peroxidase labeled nanobody VHH9 (VHH9-HRP) between free parathion and parathion hapten 1 coupled with ovalbumin (H_1-OVA) that was covalently immobilized on the activated surface of nanofibers. The assembly steps of established immunosensor were evaluated by electrochemical impedance spectra (EIS) and fourier transform infrared spectroscopy (FTIR), and its sensitivity, specificity, reusability and stability performances were investigated under optimal assay condition. Moreover, the proposed immunosensor was used for parathion quantification in spiked food samples, and its accuracy was validated using ultra performance liquid chromatography (UPLC) as well.

2. Materials and methods

2.1. Materials

The H_1-OVA and VHH9 were prepared by our laboratory (Xu et al., 2009; Zhang et al., 2018). Parathion and other O, O-diethyl organophosphorus pesticides standards were purchased from Dr. Ehrenstorfer GmbH (Augsburg, Germany). SPCE was obtained from Zensor R&D Co. Ltd (Taiwan, China). Silver conductive paint (SCP) was obtained from Guangzhou Kaixiang Electronics Co. Ltd. (Guangzhou, China). Hydroquinone (HQ) and hydrogen peroxide (H_2O_2) were purchased from Guangzhou Chemical Reagent Co. Ltd. (Guangzhou, China). HRP was purchased from Macklin Biochemical Technology Co. Ltd. (Shanghai, China). PVA, bovine serum albumin (BSA) and *N*-hydroxysuccinimide (NHS) were obtained from Aladdin Reagents Co. Ltd. (Shanghai, China). 1-(3-Dimethylaminopropyl)-3-ethylcabodiimide hydrochloride (EDC) was purchased from Saen Chemical Reagent Co. Ltd. (Shanghai, China). Sodium borohydride ($NaBH_4$) and sodium periodate ($NaIO_4$) were purchased from Tianjin Fuchen Chemical Reagent Co. Ltd. (Tianjin, China). CA was obtained from Sigma-Aldrich Co. Ltd. (Shanghai, China).

2.2. Preparation and characterization of PVA/CA NFM

First, PVA solutions with concentrations of 14%, 16% and 18% were prepared by constantly stirring at 80°C for 2 h, and CA was added to the PVA solutions at 10%, 15% and 20% (wt./PVA weight) under constant stirring for 30 min. The viscosity and conductivity of the electrospinning solutions were measured in a viscometer (LV-SSR, FANGRUI, China) and a conductivity meter (DDS-11A, China), respectively. Electrospinning was carried out at a voltage of 16–20 kV, an injection rate of 0.15–0.55 mL/h and a distance of 13–17 cm. PVA/CA NFM was prepared at 25 ± 2°C and 60 ± 2% relative humidity, and followed by heat-treatment to initiate cross-linking. The corresponding cross-linked PVA/CA casting membrane (PVA/CA CM) was also fabricated.

The morphologies of PVA/CA NFM under different steps of immunosensor assembly process were investigated by scanning electron microscope (SEM, Merlin, ZEISS, German). The contact angle analyzer (Data Physics Instruments, OCA 20, Germany) was applied for measuring the water contact angle (WCA) of cross-linked PVA/CA NFM. The FTIR of PVA/CA NFM and individual compounds were measured with a VERTEX 70 FTIR Spectrometer (Bruker Co., Ettlingen, Germany) in the scanning region of 400–3800 cm^{-1}. In which, ATR was adopted for PVA/CA NFM, while KBr disk was selected for individual compounds.

2.3. Construction of the electrochemical immunosensor

The cross-linked PVA/CA NFM modified SPCE was fabricated by laminating a 3 mm cross-linked PVA/CA NFM plate with 0.1 mm thickness on the working electrode of SPCE using SCP. Then, 100 μL of 1 mM EDC/NHS was dropped onto the electrode at 4°C for 2 h for activation of carboxyl groups. After being rinsed with PBS, the electrode was incubated with 10 μL of H_1-OVA at 4°C for 2 h, and followed by rinsing again with PBS to the remove unbound H_1-OVA. Afterwards, the remaining active sites were blocked with 100 μL of 1%BSA. Finally, the BSA/H_1-OVA/PVA/CA NFM/SCP/SPCE was sealed and stored at 4°C after washing with PBS.

VHH9-HRP was prepared by sodium periodate method and the detailed synthesized process was described in supporting information. After that, the electrode was incubated with a mixture containing 5 μL of VHH9-HRP and 5 μL different concentrations of parathion at 4°C for a period. Afterwards, the surface of electrode was rinsed with PBS to remove non-captured VHH9-HRP and parathion-VHH9-HRP complex, followed by drying with nitrogen. The stepwise fabrication procedure and sensing mechanism of immunosensor were depicted in Scheme 1.

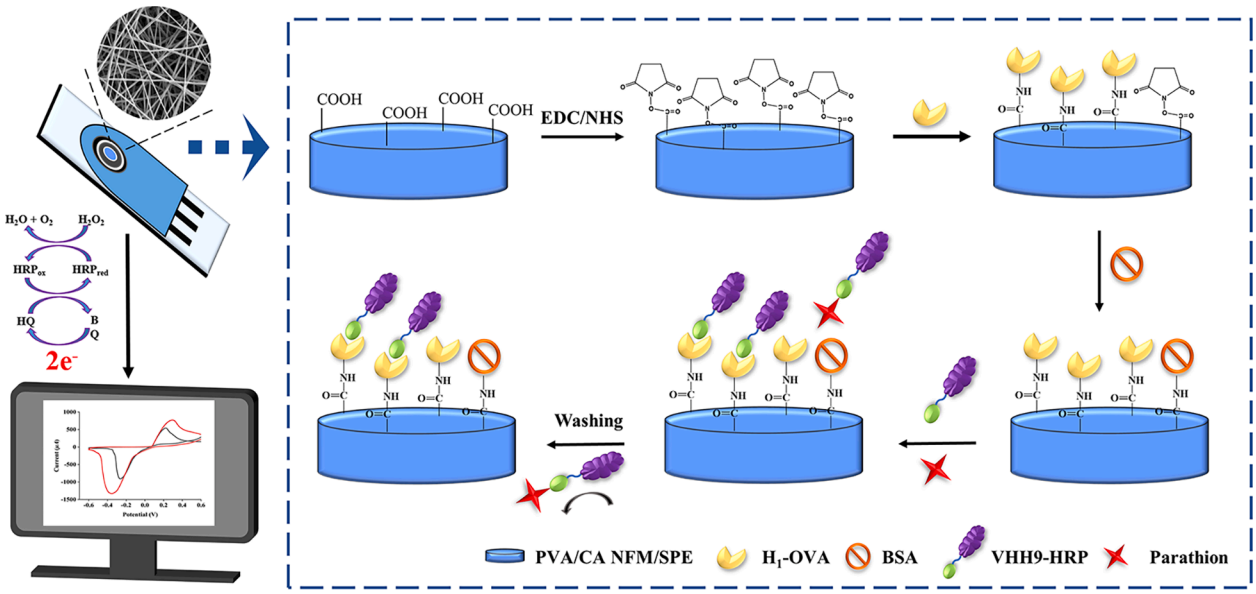

Scheme 1. Illustration of stepwise fabrication procedure and sensing mechanism of cross-linked PVA/CA NFM-based immunosensor for parathion detection.

2.4. Electrochemical measurements

Electrochemical measurement was performed by a CHI660D electrochemical work station (Shanghai Chenhua Instrument Corporation, Shanghai, China), in which, EIS was used to characterize the modification process of electrodes under the 0.1 mol/L KCl solution containing 5 mM $[Fe(CN)_6]^{3-/4-}$ solvent system. For the detection of parathion, the prepared immunosensor was dipped into 1/15 mol/mL PBS containing 0.5 mM HQ to perform cyclic voltammogram (CV) measurements in the applied potential ranging from − 0.6 V to + 0.6 V at a scanning rate of 100 mV/s. Possible catalytic mechanism of HQ/HRP/H_2O_2 system was shown in supporting information, and the change of reduction peak current (ΔI) before and after the addition of H_2O_2 was used as the signal response (Gan et al., 2016).

2.5. Specificity, reusability and stability of the electrochemical immunosensor

To evaluate the specificity of fabricated immunosensor, the cross-reactivity (CR) against five parathion analogues and their mixture were investigated under the same experimental conditions. The CR of parathion analogues was calculated by the following equation:

$$CR(\%) = \frac{\Delta I_{[blank]} - \Delta I_{[analogues]}}{\Delta I_{[blank]} - \Delta I_{[parathion]}} \times 100\%$$

where $\Delta I_{[blank]}$ represented the current response of blank measurement and $\Delta I_{[parathion]}$ and $\Delta I_{[analogues]}$ represented the current response of parathion and parathion analogues at the same concentration of 1 ng/mL, respectively (Guan et al., 2019).

For the regeneration experiment, the ΔI of original immunosensor was set as 100%, and the changes of ΔI under different concentrations of parathion (0.1, 1 and 10 ng/mL) were studied. The regeneration process was carried out as follows: after each detection of parathion, the immunosensor was dipping into a 0.1 M glycine hydrochloric acid buffer (pH 2.8) for 5 min followed by washing with PBS solution. Moreover, the several prepared immunosensors were sealed and stored at 4°C, and the stability was checked by monitoring the current response changes of immunosensor.

2.6. Analysis of parathion in food samples

The Chinese cabbage, cucumber, and orange samples were obtained from local markets in Guangzhou, China, and verified as parathion-free by UPLC. The sample pre-treatment and the spike-and-recovery experiment at five concentration levels (0.05, 0.10, 1, 5 and 10 ng/mL) were performed according to the previous report (Zhang et al., 2018). The sample extracts were diluted with PBS and followed by parathion analysis using proposed electrochemical immunosensor and UPLC, respectively.

3. Results and discussion

3.1. Preparation of PVA/CA NFM

In order to host a huge amounts of target biomolecules, the uniform PVA/CA NFM with ultra-high surface area and high porosity should be prepared (Smith et al., 2020). It was reported that the change of solution's viscosity and conductivity could result in the different morphology of nanofiber (Xiang et al., 2022). Therefore, the influence of varied concentrations of PVA and CA on the nanofiber morphology was studied by SEM. From Table 1, it can be seen that the viscosity increased from 1.534 to 3.851 Pa·S with an increase of PVA concentration, while the conductivity was almost unchanged. Spindle-like fibers were obtained under lower or higher PVA concentration and the uniform morphology with bead-free fibers at 16%PVA (Fig. S1.a–c). This can be ascribed to the fact that viscosity of 14%PVA solution was too low to form homogeneous fibers, when the concentration of PVA increased to 16%, the more intermolecular entanglement was sufficient to form stable and homogeneous fibers, and further increasing PVA concentration (18%) can counteract the stretch of fibers, thus resulting in unstable

Table 1
Solution properties and fiber average diameters of PVA/CA NFM.

PVA (%)	CA (%)	Conductivity (ms/cm)	Viscosity (Pa·S)	Average diameter (nm)
14	15	1.728 ± 0.003	1.534 ± 0.004	290
16	15	1.823 ± 0.006	2.905 ± 0.008	410
18	15	1.797 ± 0.008	3.851 ± 0.005	420
16	10	1.340 ± 0.002	2.923 ± 0.003	370
16	15	1.823 ± 0.006	2.905 ± 0.008	410
16	20	2.013 ± 0.006	2.854 ± 0.007	450

jets.

Then, different levels of CA were added to cross-link with PVA, as well as providing abundant carboxyl groups for the immobilization of coating antigen. A remarkable enhancement of conductivity was achieved when the CA concentration increased from 10% to 20% due to its electrolyte nature (Table 1), while there was a weak decreased trend of viscosity. Under the influence of viscosity and conductivity, the nanofiber showed better morphologies at 10% and 15%CA, while spindle-shaped fibers were obtained for 20%CA (Fig. S1.d–f). Hence, 16% PVA/15%CA NFM was chosen as the optimal nanofiber membrane to provide more carboxyl groups for cross-linking and antigen immobilization.

Moreover, the spinning technology parameters such as voltage, injection rate and distance also play a critical role in nanofiber morphology (Wen et al., 2016). The SEM images and fiber diameter distributions of 16 %PVA/15 %CA NFM under different conditions were shown in Fig. S2. It was observed that smooth and uniform fibers had a narrower fiber distribution ranging from 220 to 410 nm with an average diameter of 320 nm under 18 kV voltage, 0.35 mL/h injection rate and 15 cm distance.

3.2. Cross-linked PVA/CA NFM

Since the 16%PVA/15%CA NFM can be swollen in aqueous solution, a cross-linking treatment is needed. The cross-linking was attributed to the esterification reaction between PVA and CA, of which reaction mechanism was presented in Fig. S3 (Lopez-Cordoba et al., 2016). Firstly, the effects of cross-linking temperature on the morphology changes of cross-linked PVA/CA NFM after soaking in PBS were investigated. The thermal cross-linking caused little change on the fiber morphologies (Fig. 1.a–c), however, the morphologies of cross-linked PVA/CA NFM soaked in PBS were strikingly different depending on the cross-linking temperature (Fig. 1.d–f). The PVA/CA NFM heated at 125°C also became swollen and adhesive when soaked in PBS, relatively, the clear fibrous morphologies were obtained for cross-linking temperature reached to 145°C and 165°C. These changes were consistent with the WCA of cross-linked PVA/CA NFM, which increased from 30.12° to 59.62° with temperature increasing from 125°C to 165°C (Fig. 1.g), suggesting the enhanced water stability of cross-linked PVA/CA NFM.

On the other hand, the optimal cross-linking time was also studied. Similarly, there was almost no morphology differences of 16%PVA/15% CA NFM heated for different time (Fig. S4.a–d). However, after soaking in PBS buffer for 12 h, the PVA/CA NFM heated for 0.5 h or 1 h both showed fused film-like morphologies (Fig. S4.e–f), owing to incomplete cross-linking (Koosha et al., 2019). On the contrary, the morphologies were still uniform for 2 h and 4 h (Fig. S4.g–h), as the WCA increased to be 56.39° and 57.73°, respectively (Fig. S4.i), demonstrating that the cross-linked PVA/CA NFM possessed desired water stability. Since CA cross-linking was demonstrated to cause yellowing under elevated temperatures or longer time (Shi & Yang, 2015), the cross-linking reaction was completed at 145°C for 2 h.

3.3. Construction of the electrochemical immunosensor

The cross-linked PVA/CA NFM was utilized as the modified electrode material for covalently immobilizing biomolecules (H_1-OVA, coating antigen), and the parathion determination was achieved via a typical competition for binding to VHH9-HRP between free parathion and H_1-OVA. In which, the VHH9-HRP was prepared successfully and its UV–vis spectra and ELISA results were shown in Fig. S5.

3.3.1. Structural and morphology characterization

FTIR was used to characterize the ester groups formation in cross-linking reaction and the successful immobilization of H_1-OVA on the cross-linked PVA/CA NFM. From Fig. S6, the characteristic peaks for PVA at 3332 cm^{-1}, 2941 cm^{-1}, 1430 cm^{-1} and 1092 cm^{-1} were corresponding to O—H stretching, C—H stretching, C—H_2 bending and —C—O stretching, respectively. The peak at 1734 cm^{-1} was ascribed to C═O stretching from residual acetyl groups of PVA (curve a) (Mansur et al., 2008; Sabzi et al., 2020). For CA, the band at 1750 cm^{-1} was assigned to the carboxyl groups (curve b). In the spectra of PVA/CA NFM (curve c), the O—H stretching vibration absorption band was shifted to a lower frequency, which was attributed to the formation of hydrogen bonds, indicating the good compatibility between PVA and CA (Wang et al., 2014). Moreover, a reduction of the peak assigned to hydroxyl groups was showed in the FTIR of cross-linked PVA/CA NFM (curve d), demonstrating that hydroxyl groups participated in cross-linking. Additionally, a new peak appeared at 1027 cm^{-1} was ascribed to a characteristic band of C—O—C from aliphatic ester groups, and the band at 1718 cm^{-1} was ascribed to the C═O stretching, which may be a coalescence peak generated by the ester bond and residual carboxyl C═O groups of CA (Sabzi et al., 2020). These peaks indicated the successful cross-linking between PVA and CA (Lopez-Cordoba et al., 2016; Suganthi et al., 2018). Then, the residual carboxyl groups of cross-linked PVA/CA NFM were activated with EDC/NHS for covalently immobilization of H_1-OVA, two new peaks appeared at 1654 cm^{-1} and 1590 cm^{-1} were corresponded to the C═O stretching vibration of the amide I band and the N—H bending vibration of amide II bands, respectively (curve e) (Basturk et al., 2013). The results demonstrated the successful immobilization of H_1-OVA on cross-linked PVA/CA NFM by the formation of amide bonds between amine groups of H_1-OVA and carboxyl groups on cross-linked PVA/CA NFM.

Then, the morphologies of cross-linked PVA/CA NFM under different steps of immunosensor assembly process were also characterized. The

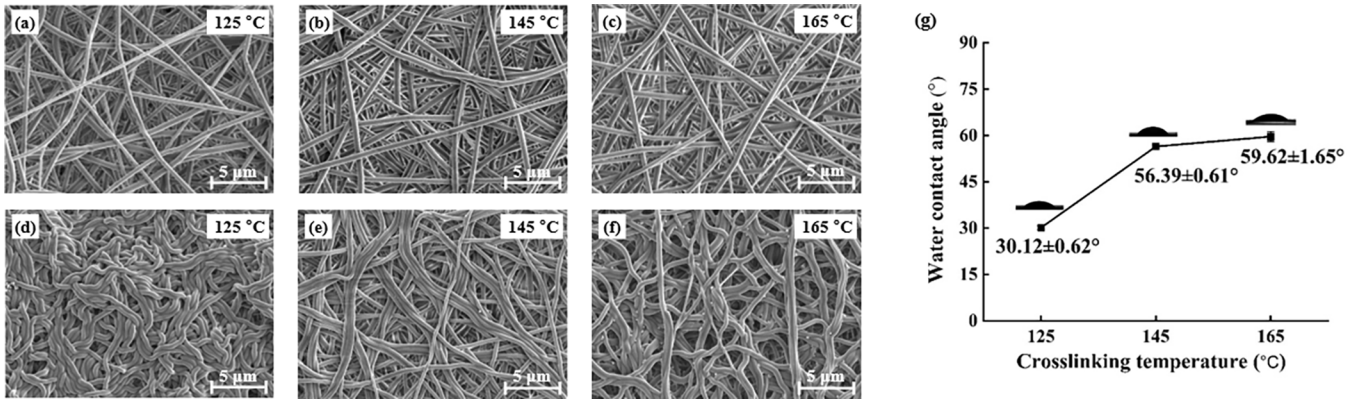

Fig. 1. SEM images of cross-linked 16%PVA/15%CA NFM under different cross-linking temperature (a–c) and after soaking in PBS for 12 h (d–f), the WCA of cross-linked 16%PVA/15%CA NFM under different cross-linking temperature (g).

pristine PVA/CA NFM possessed nonwoven membrane structures (Fig. S7.a), after heating at 145°C for 2 h, the nanofiber morphology remained unchanged (Fig. S7.b). By activation with EDC/NHS, cross-linked PVA/CA NFM became swollen with the average diameter increasing from 400 to 470 nm (Fig. S7.c), which could be attributed to hydrophilic properties of remaining hydroxyl and carboxyl groups on the nanofibers (Shi & Yang, 2015). Subsequently, the further increased average diameters of nanofibers and adhesion between nanofibers were observed after H_1-OVA immobilization, BSA blocking and incubation with VHH9-HRP, respectively (Fig. S7.d–f). These results were possibly ascribed to the enhancement in the attraction among fibers through hydrogen-bond formation with biomolecules, evidencing of successful biomolecules immobilization onto nanofibers (Chauhan & Solanki, 2019). On the other hand, the cross-linked PVA/CA NFM still retained micro-porosity and nanofibrous structures, revealing its structural stability and practicability, ensuring it can be an ideal modified electrode material for the electrochemical immunosensor.

3.3.2. *Electrochemical characterization*

EIS was adopted to demonstrate the successful assembly of immunosensor, as it can offer detailed information on capacitance/resistance changes at the surface-electrolyte interface caused by layer-by-layer assembly on electrode surface. A common electronic equivalent circuit in the inset of Fig. 2.A was used to model interfacial phenomena, consisting of the electrolyte resistance (R_s), Warburg impedance (Z_w), the capacitance of the double layer (C_{dl}) and the electron-transfer resistance (R_{et}). In which, R_{et} reflects the electron transfer kinetics of the redox probe at the electrode interface, its value can change with the electrode modification and the interaction between electrode surface and the electrolyte, which can be extracted from a semicircle portion of impedance spectra presented in the form of Nyquist plot (Katz & Willner, 2003). As shown in Fig. 2.A, the R_{et} of SCP/SPCE (curve b; 239.80 Ω) was lower than that of bare SPCE (curve a; 274.46 Ω) due to the good conductivity of SCP. Further modification of SCP/SPCE with the cross-linked PVA/CA CM showed a great increase in R_{et} (curve c, 4702 Ω), while it was decreased by more than 10 times with the replacement of CM by cross-linked PVA/CA NFM (curve d, 436.77 Ω), indicating faster diffusion of electrons at electrode–electrolyte interface was occurred for cross-linked PVA/CA NFM due to its porous structure, making nanofiber as a promising modified electrode material for establishing sensing systems with high sensitivity. Similarly, El-Moghazy et al. found that the modification of poly(vinyl alcohol-co-ethylene) (PVA-*co*-PE) NFM on the SPCE caused a decrease of the electron-transfer resistance by about 4 times in comparison with the PVA-*co*-PE CM (El-Moghazy et al., 2018). After the immobilization of H_1-OVA and BSA onto cross-linked PVA/CA NFM/SCP/SPCE, the R_{et} was further enhanced as the immobilized biomolecules could hinder electron transfer, which was also the evidence for the successful immobilization on the electrode (curve e, 885.77 Ω; curve f, 1280 Ω). The deterred electron transfer continued with the incubation of VHH9-HRP (curve g, 1478 Ω), indicating the antigen–antibody complex caused a limitation of the electron transfer. The obtained EIS results confirmed the successful assembly of the immunosensor. Similar results by Chauhan's study also proved the successful assembly of cellulose acetate fiber-based biosensor, as R_{et} value increased from 2.78 to 4.24 kΩ after the immobilization of antibody and BSA (Chauhan & Solanki, 2019).

3.4. *Optimization of the determination conditions*

For purpose of achieving the best analytical performance of the immunosensor, the effects of five important determination conditions were examined by measuring Δ*I* using CV, including the concentration and immobilization time of H_1-OVA, the concentration of VHH9-HRP, immuno-reaction time, the concentration of H_2O_2. Single factor analysis was employed to investigate the optimal value of above five factors. Generally, an increase in the number of H_1-OVA could combine with a larger number of VHH9-HRP, resulting in higher current response. It can be seen that the Δ*I* increased with increasing the concentration of H_1-OVA from 2.5 to 5 μg/mL and then decreased when further increasing the concentration of H_1-OVA (Fig. 2.B). The results may be ascribed to

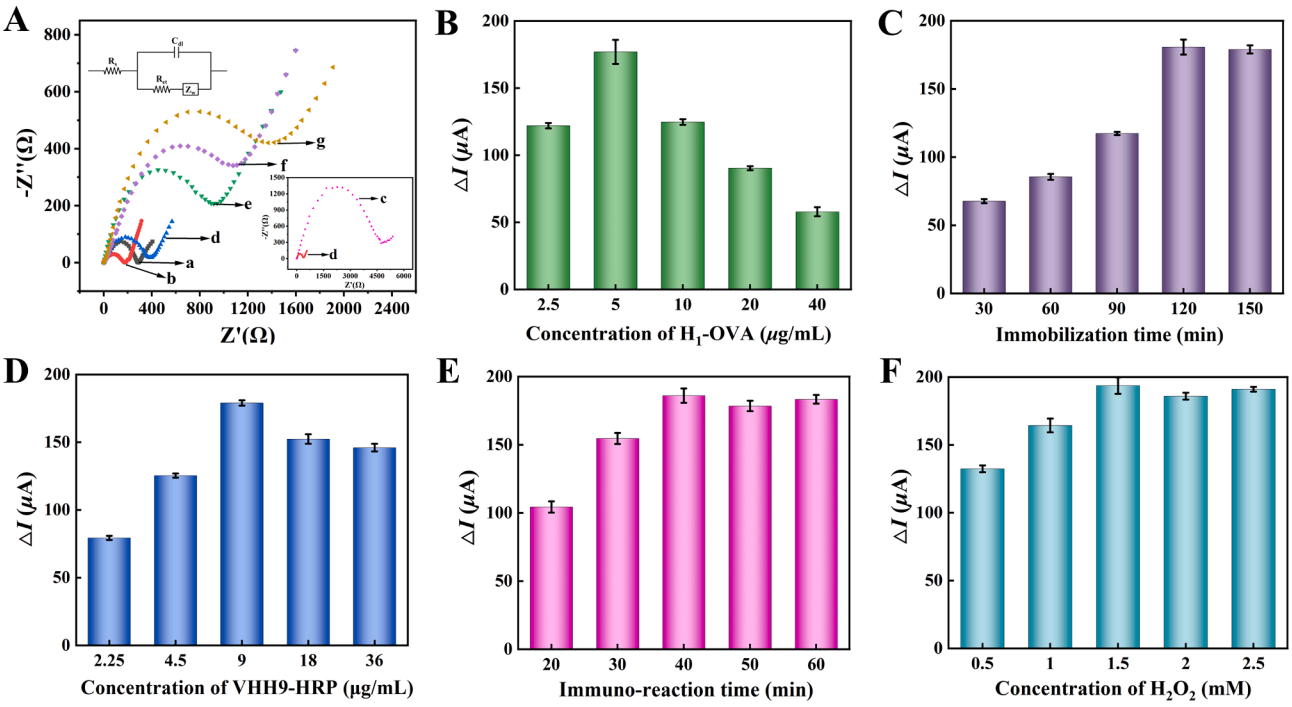

Fig. 2. (A) The Nyquist plots for bare SPCE (curve a), SCP/SPCE (curve b), cross-linked PVA/CA CM/SCP/SPCE (curve c), cross-linked PVA/CA NFM/SCP/SPCE (curve d), H_1-OVA/PVA/CA NFM/SCP/SPCE (curve e), BSA/H_1-OVA/PVA/CA NFM/SCP/SPCE (curve f), VHH9-HRP/BSA/H_1-OVA/PVA/CA NFM/SCP/SPCE (curve g); optimization of the determination conditions: (B) concentration of H_1-OVA; (C) immobilization time of H_1-OVA; (D) concentration of VHH9-HRP; (E) immuno-reaction time and (F) concentration of H_2O_2 (Error bars = RSD, n = 3).

the steric hindrance formed by higher density of H_1-OVA, which prevented the binding of VHH9-HRP to H_1-OVA and the electron transfer (Chauhan et al., 2018). Subsequently, the immobilization time of H_1-OVA was also investigated. The ΔI increased gradually with an increase of immobilization time and then achieved its plateau at 120 min (Fig. 2.C), revealing the immobilization sites of cross-linked PVA/CA NFM have been saturated (El-Moghazy et al., 2020). Hence, 120 min was chosen as the optimum immobilization time for 5 μg/mL H_1-OVA. In addition, the concentration of VHH9-HRP was also considered as the one of critical factors that affected the sensitivity of immunosensor. It was observed that the ΔI was proportional to the concentration of VHH9-HRP at the range from 2.25 to 9 μg/mL and then decreased slightly (Fig. 2.D), which was due to the fact that the excess VHH9-HRP cannot completely combine with the H_1-OVA because of steric-hindrance, and moreover, the interaction between antigen and antibody need some time to achieve equilibrium (Chauhan et al., 2018). In addition, with the increase of antigen–antibody immuno-reaction time, the ΔI enhanced accordingly and tended to be stable at 40 min (Fig. 2.E), as too long immuno-reaction time could affect the binding ability between antigen and antibody (Dong et al., 2017). Finally, the concentration of H_2O_2 was also explored since it had a significant impact on the enzyme-catalyzed reaction and the biomolecule activity, and the ΔI increased gradually with increasing H_2O_2 concentration and then decreased, as antigen–antibody interaction and HRP activity may be influenced under the strong oxidation of higher H_2O_2 concentration (Li et al., 2018; Zhang et al., 2019), so the optimal concentration of H_2O_2 was 1.5 mM (Fig. 2.F).

3.5. Analytical performance of the electrochemical immunosensor

Under optimum experimental conditions, the standard calibration curve was established as illustrated in Fig. 3.A. The ΔI decreased proportionally with increasing concentration of parathion and the linear regression equation was as following: ΔI (μA) = (126.83 ± 0.45) − (33.23 ± 0.29) Log $C_{parathion}$ (ng/mL) (R^2 = 0.9995). The LOD was 2.26 pg/mL (LOD = Y + 3SD, where Y is the average of blank measurement, SD is the standard derivation of blank measurement). In comparison with the performances of other analytical methods for parathion (Table S1), the immunosensor modified by cross-linked PVA/CA NFM exhibited desirable sensitivity, long-term stability, low cost and simple preparation for the determination of parathion, demonstrating that the nanofiber with porous structure was beneficial for biomolecules reaching recognition sites and provided a fast channel for the electron transfer.

3.6. Specificity, reusability and stability of the electrochemical immunosensor

To investigate the specificity of designed immunosensor, the CR against five parathion analogues and their mixture, including triazophos, quinaphos, coumaphos, phorate and phoxim, were calculated under the same experimental conditions. The CRs to triazophos, quinalphos and coumaphos were 11.31%, 9.46% and 5.31%, respectively, especially, the CRs to phorate, phoxim and their mixture were lower than 0.3% (Fig. 3.B), which confirmed that the proposed immunosensor presented good specificity to parathion. These results were similar with that of VHH9-AP based dc-FEIA, as the CRs of which to triazophos, quinalphos, and coumaphos were 8.0%, 6.5%, and 4.9%, respectively, and CRs to other parathion analogues were lower than 0.6% (Zhang et al., 2018).

The reusability should also be considered for developing a practical

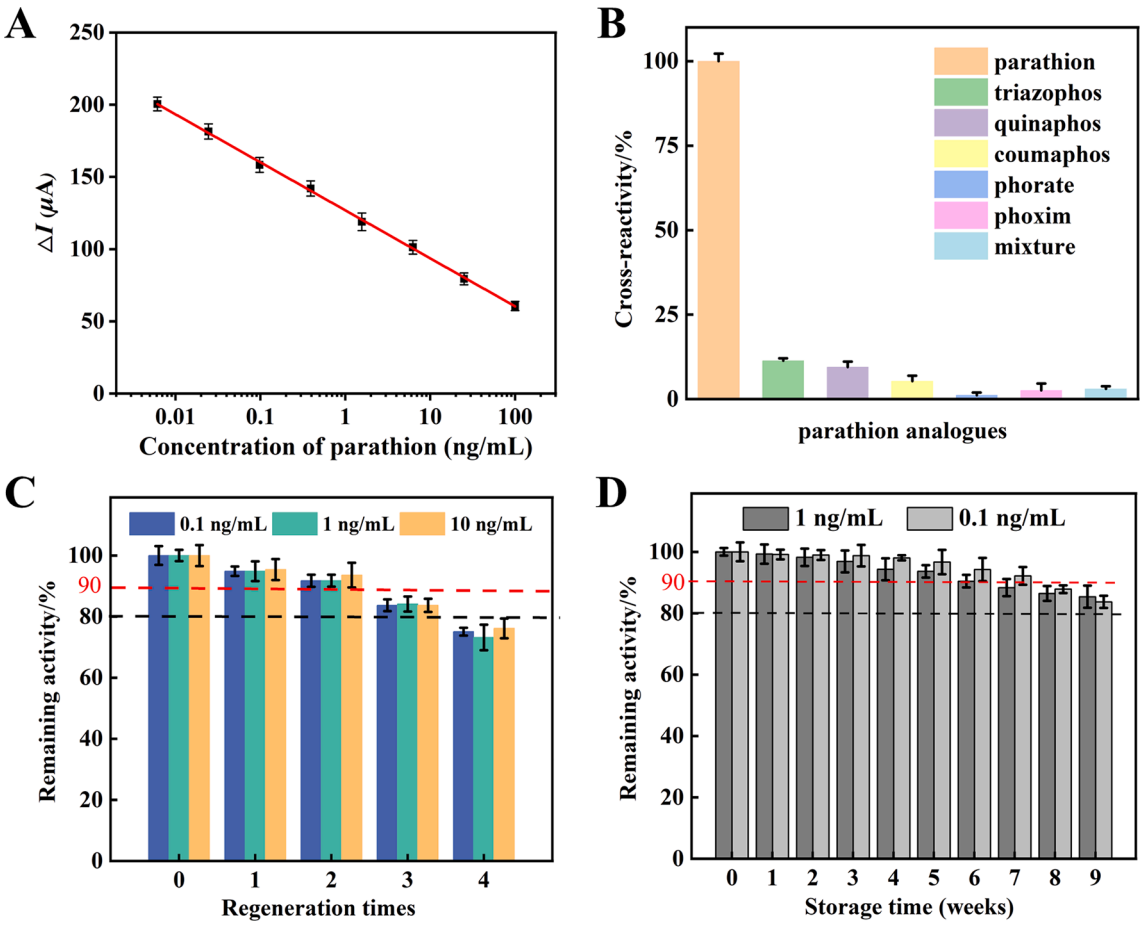

Fig. 3. (A) Standard curve; (B) specificity; (C) reusability and (D) stability of the electrochemical immunosensor (Error bars = RSD, n = 3).

immunosensor. The CV curves for the regeneration of immunosensor were shown in Fig. S8, including CV curves before and after the addition of H_2O_2. For the regeneration experiment, the ΔI of original immunosensor was set as 100%, and the changes of ΔI under different concentration of parathion (0.1, 1 and 10 ng/mL) were studied (El-Moghazy et al., 2020). Results showed that the regenerated immunosensor still kept more than 90% of its initial activity in the first two times regeneration and about 85% after regenerating 3 times, and less than 75% after regenerating 4 times (Fig. 3.C), meaning the immunosensor that have been regenerated 3 times still have the ability to detect different concentrations of parathion. The decrease of ΔI may be attributed to protein degeneration and spoilage of cross-linked PVA/CA NFM during regeneration steps (El-Moghazy et al., 2018). Similar phenomenon was also reported in the El-Moghazy's study, which reported that the biosensor based on decorated nylon 6 nanofibrous membranes maintained more than 90% of its initial activity in the first regeneration and about 66% after regenerating 2 times under the 0.1 ng/mL of 3-Phenoxybenzoic acid (El-Moghazy et al., 2020).

Moreover, the immunosensor's stability was also studied under two concentrations of parathion (0.1 and 1 ng/mL, respectively). The ΔI of original immunosensor for detection to parathion was set as 100%, it can be seen that the immunosensor was retained almost 100% after 3 weeks of storage, around 90% and 85% after 6 weeks and 9 weeks, respectively (Fig. 3.D). The long-term stability of fabricated immunosensor could be attributed to good stability and biocompatibility of cross-linked PVA/CA NFM that protected the activity of biomolecules. Similar with this study, Au nanoparticles/polyethyleneimine/carbon nanofibers-based immunosensor remained 97.25% and 94.39% after 3 and 6 days of storage, respectively, and less than 90% after 12 days (Huang et al., 2021).

3.7. Applicability of the electrochemical immunosensor

In order to assess the applicability of proposed immunosensor, three food samples (cucumber, orange and Chinese cabbage) that spiked with different concentrations of parathion (1, 5 and 10 ng/g) were analyzed by the fabricated immunosensor and UPLC, respectively. From Table 2, it can be seen that the average recoveries by both methods were 96.20%–114.61% and 76.30%–105.60% with the coefficient of variation (CV) of 1.06%–5.28% and 1.25%–11.80%, respectively, showing a good consistency between spiked and recovered levels of parathion. Moreover, the related coefficient (R^2) of above two methods was 0.9964 (Fig. S9), suggesting that precision and accuracy of proposed immunosensor were almost consistent with UPLC.

Moreover, the food samples spiked with two low concentrations of parathion (0.05 and 0.10 ng/g) were analyzed by the proposed immunosensor. Table 2 showed that the average recoveries were 89.15%–116.13% with CV ranging from 1.83% to 10.92%, indicating the high sensitivity for parathion in spiked food samples. However, the food samples spiked with these two concentrations of parathion were not detected by the UPLC, since these two levels were below the detection limit of UPLC, and the corresponding recoveries and CV cannot be obtained. These results indicated that the established immunosensor was accurate to use in spiked food samples, suggesting its potential application in monitoring the parathion residues levels of contaminated samples.

4. Conclusions

In conclusion, a simple electrochemical immunosensor with high sensitivity was successfully developed for the quantification of parathion by using VHH9-HRP and the cross-linked PVA/CA NFM modified SPCE. The cross-linked PVA/CA NFM possessed unique characteristic and ideal water stability, providing an appropriate microenvironment for the immobilization of biomolecules and a porous structure for the fast transfer of electrons. The established immunosensor exhibited high sensitivity and strong selectivity for parathion with the LOD of 2.26 pg/mL. Furthermore, the good stability and reusability of the designed immunosensor were also demonstrated, as well as desirable accuracy and sensitivity for the detection of parathion in spiked food samples compared to UPLC. These results proved the potential of nanofiber as modified electrode material for electrochemical immunosensor, and the newly developed immunosensor was a reliable sensing platform for the sensitive and selective determination of parathion.

CRediT authorship contribution statement

Wen-jia Yin: Investigation, Validation, Formal analysis, Writing – original draft, Writing – review & editing. **Jing-xian Zhang:**

Table 2
Comparison of electrochemical immunosensor with UPLC for detecting parathion in spiked food samples (n = 3).

Real samples	Spiked (ng/g)	Electrochemical immunosensor			UPLC		
		Mean ± SD[a] (ng/g)	Recovery (%)	CV[b] (%)	Mean ± SD[a] (ng/g)	Recovery (%)	CV[b] (%)
Cucumber	0.00	ND[c]	/	/	ND[c]	/	/
	0.05	0.05 ± 0.00	102.63	1.83	ND[c]	/	/
	0.10	0.12 ± 0.01	116.13	6.93	ND[c]	/	/
	1.00	1.12 ± 0.02	112.26	1.44	0.92 ± 0.06	94.70	6.35
	5.00	5.02 ± 0.26	100.35	5.28	4.56 ± 0.54	91.27	11.80
	10.00	11.46 ± 0.24	114.61	2.12	10.56 ± 1.05	105.60	9.96
Orange	0.00	ND[c]	/	/	ND[c]	/	/
	0.05	0.05 ± 0.00	89.15	2.13	ND[c]	/	/
	0.10	0.10 ± 0.00	102.88	4.04	ND[c]	/	/
	1.00	1.00 ± 0.04	96.65	3.95	0.76 ± 0.07	76.30	9.45
	5.00	4.92 ± 0.05	98.43	1.06	5.13 ± 0.10	102.68	1.87
	10.00	10.21 ± 0.25	102.12	2.49	9.95 ± 0.26	99.53	2.64
Chinese cabbage	0.00	ND[c]	/	/	ND[c]	/	/
	0.05	0.05 ± 0.01	100.00	10.92	ND[c]	/	/
	0.10	0.10 ± 0.00	98.42	2.08	ND[c]	/	/
	1.00	1.06 ± 0.05	105.54	4.67	0.87 ± 0.01	86.70	1.25
	5.00	4.81 ± 0.13	96.20	2.60	4.68 ± 0.44	93.59	9.49
	10.00	10.00 ± 0.18	100.01	1.82	9.91 ± 0.40	99.14	4.08

[a] Standard deviation.
[b] Coefficient of variation.
[c] Not detected.

Methodology, Formal analysis. **Hong Wang:** Methodology, Supervision, Funding acquisition. **Yu Wang:** Validation. **Xi Zeng:** Validation. **Zhenlin Xu:** Methodology. **Jin-yi Yang:** Conceptualization. **Zhi-li Xiao:** Conceptualization. **Bruce D. Hammock:** Supervision. **Peng Wen:** Investigation, Validation, Formal analysis, Writing – original draft, Writing – review & editing.

Declaration of Competing Interest

The authors declare that they have no known competing financial interests or personal relationships that could have appeared to influence the work reported in this paper.

Data availability

Data will be made available on request.

Acknowledgments

This work was supported by Lingnan Modern Agricultural Science and Technology Guangdong Laboratory Independent Scientific Research Project (NZ2021032), National Natural Science Foundation of China (31972157), Science and Technology Planning Project of Guangzhou City (202102080615), Guangdong Province Universities and Colleges Pearl River Scholar Funded Scheme 2017, Guangdong Provincial Key Laboratory of Food Quality and Safety (2020B1212060059).

Appendix A. Supplementary data

Supplementary data to this article can be found online at https://doi.org/10.1016/j.foodchem.2022.134371.

References

Basturk, E., Demir, S., Danis, O., & Kahraman, M. V. (2013). Covalent immobilization of a-amylase onto thermally crosslinked electrospun PVA/PAA nanofibrous hybrid membranes. *Journal of Applied Polymer Science, 127*(1), 349–355. https://doi.org/10.1002/app.37901

Chauhan, D., Gupta, P. K., & Solanki, P. R. (2018). Electrochemical immunosensor based on magnetite nanoparticles incorporated electrospun polyacrylonitrile nanofibers for vitamin D_3 detection. *Materials Science & Engineering C-Materials for Biological Applications, 93*, 145–156. https://doi.org/10.1016/j.msec.2018.07.036

Chauhan, D., & Solanki, P. R. (2019). Hydrophilic and insoluble electrospun cellulose acetate fiber-based biosensing platform for 25-hydroxy vitamin-D_3 detection. *ACS Applied Polymer Materials, 1*(7), 1613–1623. https://doi.org/10.1021/acsapm.9b00179

Chen, G., Jin, M., Du, P., Zhang, C., Cui, X., Zhang, Y., … Wang, J. (2017). A sensitive chemiluminescence enzyme immunoassay based on molecularly imprinted polymers solid-phase extraction of parathion. *Analytical Biochemistry, 530*, 87–93. https://doi.org/10.1016/j.ab.2017.05.008

Dong, X. X., Yang, J. Y., Luo, L., Zhang, Y. F., Mao, C., Sun, Y. M., … Xu, Z. L. (2017). Portable amperometric immunosensor for histamine detection using prussian blue-chitosan-gold nanoparticle nanocomposite films. *Biosensors & Bioelectronics, 98*, 305–309. https://doi.org/10.1016/j.bios.2017.07.014

El-Moghazy, A. Y., Huo, J., Amaly, N., Vasylieva, N., Hammock, B. D., & Sun, G. (2020). An innovative nanobody-based electrochemical immunosensor using decorated nylon nanofibers for point-of-care monitoring of human exposure to pyrethroid insecticides. *ACS Applied Materials & Interfaces, 12*(5), 6159–6168. https://doi.org/10.1021/acsami.9b16193

El-Moghazy, A. Y., Zhao, C., Istamboulie, G., Amaly, N., Si, Y., Noguer, T., & Sun, G. (2018). Ultrasensitive label-free electrochemical immunosensor based on PVA-co-PE nanofibrous membrane for the detection of chloramphenicol residues in milk. *Biosensors & Bioelectronics, 117*, 838–844. https://doi.org/10.1016/j.bios.2018.07.025

Felix, F. S., & Angnes, L. (2018). Electrochemical immunosensors-a powerful tool for analytical applications. *Biosensors & Bioelectronics, 102*, 470–478. https://doi.org/10.1016/j.bios.2017.11.029

Gan, C., Ling, L., He, Z., Lei, H., & Liu, Y. (2016). In-situ assembly of biocompatible core-shell hierarchical nanostructures sensitized immunosensor for microcystin-LR detection. *Biosensors & Bioelectronics, 78*, 381–389. https://doi.org/10.1016/j.bios.2015.11.072

Guan, T., Huang, W., Xu, N., Xu, Z., Jiang, L., Li, M., … Lei, H. (2019). Point-of-need detection of microcystin-LR using a smartphone-controlled electrochemical analyzer. *Sensors and Actuators B-Chemical, 294*, 132–140. https://doi.org/10.1016/j.snb.2019.05.028

Halicka, K., & Cabaj, J. (2021). Electrospun nanofibers for sensing and biosensing applications-a review. *International Journal of Molecular Sciences, 22*(12), 6357. https://doi.org/10.3390/ijms22126357

He, Y., Ren, Y., Guo, B., Yang, Y., Ji, Y., Zhang, D., … Wang, H. (2020). Development of a specific nanobody and its application in rapid and selective determination of salmonella enteritidis in milk. *Food Chemistry, 310*, 125942. https://doi.org/10.1016/j.foodchem.2019.125942

Huang, Y., Zhu, F., Guan, J., Wei, W., & Zou, L. (2021). Label-free amperometric immunosensor based on versatile carbon nanofibers network coupled with Au nanoparticles for aflatoxin B_1 detection. *Biosensors-Basel, 11*(1), 5. https://doi.org/10.3390/bios11010005

Jain, U., Saxena, K., Hooda, V., Balayan, S., Singh, A. P., Tikadar, M., & Chauhan, N. (2022). Emerging vistas on pesticides detection based on electrochemical biosensors-an update. *Food Chemistry, 371*, 131126. https://doi.org/10.1016/j.foodchem.2021.131126

Katz, E., & Willner, I. (2003). Probing biomolecular interactions at conductive and semiconductive surfaces by impedance spectroscopy: Routes to impedimetric immunosensors, DNA-sensors, and enzyme biosensors. *Electroanalysis, 15*(11), 913–947. https://doi.org/10.1002/elan.200390114

Khairy, M., Ayoub, H. A., & Banks, C. E. (2018). Non-enzymatic electrochemical platform for parathion pesticide sensing based on nanometer-sized nickel oxide modified screen-printed electrodes. *Food Chemistry, 255*, 104–111. https://doi.org/10.1016/j.foodchem.2018.02.004

Koosha, M., Raoufi, M., & Moravvej, H. (2019). One-pot reactive electrospinning of chitosan/PVA hydrogel nanofibers reinforced by halloysite nanotubes with enhanced fibroblast cell attachment for skin tissue regeneration. *Colloids and Surfaces B-Biointerfaces, 179*, 270–279. https://doi.org/10.1016/j.colsurfb.2019.03.054

Li, F., Li, Y., Feng, J., Gao, Z., Lv, H., Ren, X., & Wei, Q. (2018). Facile synthesis of MoS_2@Cu_2O-Pt nanohybrid as enzyme-mimetic label for the detection of the Hepatitis B surface antigen. *Biosensors & Bioelectronics, 100*, 512–518. https://doi.org/10.1016/j.bios.2017.09.048

Liu, B., Gong, H., Wang, Y., Zhang, X., Li, P., Qiu, Y., … Zhang, C. (2018). A gold immunochromatographic assay for simultaneous detection of parathion and triazophos in agricultural products. *Analytical Methods, 10*(4), 422–428. https://doi.org/10.1039/c7ay02481a

Liu, B., Li, P., Wang, Y., Guo, Y., Zhang, H., Dong, S., … Zhang, C. (2020). Quantum dot submicrobead-based immunochromatographic assay for the determination of parathion in agricultural products. *Food Analytical Methods, 13*(9), 1736–1745. https://doi.org/10.1007/s12161-020-01796-2

Lopez-Cordoba, A., Castro, G. R., & Goyanes, S. (2016). A simple green route to obtain poly(vinyl alcohol) electrospun mats with improved water stability for use as potential carriers of drugs. *Materials Science & Engineering C-Materials for Biological Applications, 69*, 726–732. https://doi.org/10.1016/j.msec.2016.07.058

Mano, F., Aroso, I. M., Barreiros, S., Borges, J. P., Reis, R. L., Duarte, A. R. C., & Paiva, A. (2015). Production of poly(vinyl alcohol) (PVA) fibers with encapsulated natural deep eutectic solvent (NADES) using electrospinning. *ACS Sustainable Chemistry & Engineering, 3*(10), 2504–2509. https://doi.org/10.1021/acssuschemeng.5b00613

Mansur, H. S., Sadahira, C. M., Souza, A. N., & Mansur, A. A. P. (2008). FTIR spectroscopy characterization of poly (vinyl alcohol) hydrogel with different hydrolysis degree and chemically crosslinked with glutaraldehyde. *Materials Science & Engineering, C: Biomimetic and Supramolecular Systems, 28*(4), 539–548. https://doi.org/10.1016/j.msec.2007.10.088

Pan, D., Li, G., Hu, H., Xue, H., Zhang, M., Zhu, M., … Shen, Y. (2018). Direct immunoassay for facile and sensitive detection of small molecule aflatoxin B_1 based on nanobody. *Chemistry-A European Journal, 24*(39), 9869–9876. https://doi.org/10.1002/chem.201801202

Sabzi, M., Afshari, M. J., Babaahmadi, M., & Shafagh, N. (2020). pH-dependent swelling and antibiotic release from citric acid crosslinked poly(vinyl alcohol) (PVA)/nano silver hydrogels. *Colloids and Surfaces B-Biointerfaces, 188*, 110757. https://doi.org/10.1016/j.colsurfb.2019.110757

Sapountzi, E., Braiek, M., Chateaux, J. F., Jaffrezic-Renault, N., & Lagarde, F. (2017). Recent advances in electrospun nanofiber interfaces for biosensing devices. *Sensors, 17*(8), 1887. https://doi.org/10.3390/s17081887

Shi, J., & Yang, E. (2015). Green electrospinning and crosslinking of polyvinyl alcohol/citric acid. *Journal of Nano Research, 32*, 32. https://doi.org/10.4028/www.scientific.net/JNanoR.32.32

Singh, A., Pasha, S. K., Manickam, P., & Bhansali, S. (2016). Single-domain antibody based thermally stable electrochemical immunosensor. *Biosensors & Bioelectronics, 83*, 162–168. https://doi.org/10.1016/j.bios.2016.04.054

Smith, S., Goodge, K., Delaney, M., Struzyk, A., Tansey, N., & Frey, M. (2020). A comprehensive review of the covalent immobilization of biomolecules onto electrospun nanofibers. *Nanomaterials, 10*(11), 2142. https://doi.org/10.3390/nano10112142

Suganthi, S., Mohanapriya, S., Raj, V., Kanaga, S., Dhandapani, R., Vignesh, S., & Sundar, J. K. (2018). Tunable physicochemical and bactericidal activity of multicarboxylic-acids-crosslinked polyvinyl alcohol membrane for food packaging applications. *ChemistrySelect, 3*(40), 11167–11176. https://doi.org/10.1002/slct.201801851

Wang, F., & Wang, H. (2022). Nanobody-Based assays for the detection of environmental and agricultural contaminants. *Methods in Molecular Biology (Clifton, N.J.), 2446*, 547–554. https://doi.org/10.1007/978-1-0716-2075-5_28

Wang, S., Ren, J., Li, W., Sun, R., & Liu, S. (2014). Properties of polyvinyl alcohol/xylan composite films with citric acid. *Carbohydrate Polymers, 103*, 94–99. https://doi.org/10.1016/j.carbpol.2013.12.030

Wen, P., Yang, Y. Y., Yin, W. J., Hu, J. C., Shen, Y. D., Wang, Y., … Hammock, B. D. (2022). Preparation of an ultrasensitive electrochemical immunosensor for the rapid

detection of 19-nortestosterone based on polyvinyl alcohol/ polyacrylic acid electrospun nanofiber mat. *Sensors and Actuators B: Chemical, 370*, 132450. https://doi.org/10.1016/j.snb.2022.132450

Wen, P., Zhu, D. H., Wu, H., Zong, M. H., Jing, Y. R., & Han, S. Y. (2016). Encapsulation of cinnamon essential oil in electrospun nanofibrous film for active food packaging. *Food Control, 59*, 366–376. https://doi.org/10.1016/j.foodcont.2015.06.005

Wu, J. H., Hu, T. G., Wang, H., Zong, M. H., Wu, H., & Wen, P. (2022). Electrospinning of PLA nanofibers: recent advances and its potential application for food packaging. *Journal of Agricultural and Food Chemistry, 70*(27), 8207-8221. 10.1021/acs.jafc.2c0261.

Xiang, H. J., Zhong, A. L., Wang, H., Xiao, L., Deng, T. R., Hu, T. G., & Wen, P. (2022). Fabrication of alkali lignin-based emulsion electrospun nanofibers for the nanoencapsulation of beta-carotene and the enhanced antioxidant property. *International Journal of Biological Macromolecules, 218*, 739–750. https://doi.org/10.1016/j.ijbiomac.2022.07.121

Xu, Z. L., Xie, G. M., Li, Y. X., Wang, B. F., Beier, R. C., Lei, H. T., … Sun, Y. M. (2009). Production and characterization of a broad-specificity polyclonal antibody for O, O-diethyl organophosphorus pesticides and a quantitative structure-activity relationship study of antibody recognition. *Analytica Chimica Acta, 647*(1), 90–96. https://doi.org/10.1016/j.aca.2009.05.025

Zhang, L., Wang, Z., Wen, Y., Shi, J., & Wang, J. (2015). Simultaneous detection of parathion and imidacloprid using broad-specificity polyclonal antibody in enzyme-linked immunosorbent assay. *Analytical Methods, 7*(1), 205–210. https://doi.org/10.1039/c4ay01818d

Zhang, L., Xie, X., Yuan, Y., Chai, Y., & Yuan, R. (2019). FeS_2-AuNPs nanocomposite as mimicking enzyme for constructing signal-off sandwich-type electrochemical immunosensor based on electroactive nickel hexacyanoferrate as matrix. *Electroanalysis, 31*(6), 1019–1025. https://doi.org/10.1002/elan.201800827

Zhang, Y. Q., Xu, Z. L., Wang, F., Cai, J., Dong, J. X., Zhang, J. R., … Wang, H. (2018). Isolation of bactrian camel single domain antibody for parathion and development of one-step dc-FEIA method using VHH-alkaline phosphatase fusion protein. *Analytical Chemistry, 90*(21), 12886–12892. https://doi.org/10.1021/acs.analchem.8b03509